Automatic Modulation Classification Architectures Based on Cyclostationary Features in Impulsive Environments

TALES V. R. O. CÂMARA[1], **ARTHUR D. L. LIMA**[1], **(Student Member, IEEE)**,
BRUNO M. M. LIMA[2], **ALUISIO I. R. FONTES**[3], **ALLAN DE M. MARTINS**[2],
AND LUIZ F. Q. SILVEIRA[1], **(Member, IEEE)**

[1]Department of Computer Engineering and Automation, Federal University of Rio Grande do Norte (UFRN), Natal 59078-970, Brazil
[2]Department of Electrical Engineering, Federal University of Rio Grande do Norte (UFRN), Natal 59078-970, Brazil
[3]Department of Information, Federal Institute of Rio Grande do Norte (IFRN), Mossoró 59900-000, Brazil

Corresponding author: Tales V. R. O. Câmara (talescamara@ufrn.edu.br)

ABSTRACT Cyclostationary analysis has several applications in communications, e.g., spectral sensing, signal parameter estimation, and modulation classification. Most of them consider the additive white Gaussian noise (AWGN) channel model, although wireless communication systems may also be subject to non-Gaussian interference and impulsive noise. In this context, the communication channel can be better modeled by heavy-tailed distributions, such as the non-Gaussian alpha-stable one. Some applications of the cyclostationary approach based on the spatial sign cyclic correlation function (SSCCF), fractional lower-order cyclic autocorrelation function (FLOCAF), and cyclic correntropy function (CCF) demonstrate that these are promising solutions for the analysis of signals in the presence of impulsive non-Gaussian noise. However, the investigation of functions above applied to digital modulation recognition in impulsive environments, and the comparison among them are topics that did not adequately explore yet. This work demonstrates that SSCCF is a particular case of the FLOCAF. Besides, a detailed analysis of the use of the FLOCAF and CCF is presented to obtain cyclostationary descriptors for the recognition of digital modulations BPSK, QPSK, 8-QAM, 16-QAM, and 32-QAM. Automatic modulation classification (AMC) architectures, based on the functions mentioned above, are also proposed. Besides, another contribution showed is that both the FLOCAF and CCF allow the symbol rate parameter estimation. The performances of AMC architectures were evaluated in the scenario with modulated signals contaminated with additive non-Gaussian alpha-stable noise. The results demonstrate that both architectures can classify signals in different contamination scenarios. However, the architecture based on the CCF is more efficient than the FLOCAF-based one.

INDEX TERMS Additive non-Gaussian alpha-stable noise, correntropy, cyclic correntropy function, cyclostationary descriptors, fractional lower-order cyclic autocorrelation function, spatial sign cyclic correlation function, digital modulations, impulsive noise, automatic modulation recognition.

I. INTRODUCTION

The purpose of automatic modulation classification (AMC) is to identify the unknown modulation format of the received noisy signal, in a short period with a hit-rate as high as possible [1], [2]. Therefore, AMC is an inter-mediate stage that exists between reception and signal demodulation.

AMC applications have arisen in military scenarios, where electronic warfare, surveillance, and threat analysis demand the recognition of signal modulations to identify adversary transmitting units, aiming at recovering the intercepted signal and jamming. Nowadays, AMC also plays an important role in commercial and civil applications,

The associate editor coordinating the review of this manuscript and approving it for publication was Ganesh Naik.

supporting the development of new paradigms of communication, e.g., cognitive radio, where the transmitter dynamically selects the signal modulation type based on channel conditions.

AMC algorithms can be classified into two different categories: likelihood-based (LB) and feature-based (FB) methods [1], [3]. The LB implementation is an optimal solution in terms of the correct classification rate. However, it is associated with high computational complexity and demands prior knowledge of statistical information of the received signal, which is usually unavailable in practice. On the other hand, although sub-optimal, the FB is both a blind (without prior information) and more straightforward to implement than the LB-based approach [1], [2], [4].

There are several classification approaches based on feature extraction, e.g., instantaneous amplitude, phase, and frequency estimation [5], [6], wavelet transform [7]–[10], use of statistical features such as higher-order moments and cumulants [11]–[14], cyclostationary analysis [2], [15]–[17], and, application of information measures such as correntropy [18]. Particularly, the cyclostationary framework can be highlighted as a powerful method for feature extraction of signals in communication systems.

For over half a century, cyclostationary analysis has been used in several fields, with emphasis on communication applications [19]. Typical operations in communication systems, e.g., modulation, multiplexing, and coding lead to the manifestation of periodic statistical moments in communication signals, which are then referred to as cyclostationary processes [20]. Classical statistical methods used in signal processing, when applied to cyclostationary signals, only allow performing a limited analysis since they consider the analyzed signal is stationary. However, techniques based on cyclostationary analysis are more suitable to process communication signals [21].

Cyclostationary analysis allows the extraction of cyclic spectral features from communication signals, also known as cyclostationary signatures, and can be efficiently used in Gaussian environments for spectral sensing [22], [23], automatic modulation recognition [23]–[25], and estimation of signal parameters [20], [23], [26].

Despite being widely used in the literature to model the additive noise in communication, the white Gaussian noise (AWGN) is a limited model when applied to wireless systems, and mobile satellite communications, since such systems are also prone to non-Gaussian interference [27]–[29] and impulsive noise [30]–[32]. In such cases, the alpha-stable distribution appropriately models the communication channels, since it describes the Gaussian and non-Gaussian environments [27], [33], [34]. However, the non-Gaussian alpha-stable distribution does not have defined the second- and higher-order moments. Therefore, in this context, the second- and higher-order cyclostationary analyses are unsuitable for feature extraction from signals in environments modeled by such distribution.

The prevalent techniques for the information processing in impulsive non-Gaussian environments are the fractional lower-order statistical analysis [35]–[38], correntropy measure [39], [40], spatial sign cyclic correlation estimation [41]–[43], fractional lower-order cyclostationary analysis [44], [45], and cyclic correntropy [21], [46], [47].

As far as the authors are aware, approaches based on the spatial sign cyclic correlation estimation and the fractional lower-order cyclostationary analysis have not yet been applied to the modulation classification issue. Besides, there is no mathematical demonstration that relates both approaches.

On the other hand, cyclic correntropy is capable of extracting cyclostationary signatures from modulated signals contaminated by impulsive noise [21], [46], with application in spectral sensing [21]. However, further investigations still must be performed in order to evaluate the performance of this technique in recognition of digital modulations in non-Gaussian impulsive environments, such as M-PSK (M-ary phase-shift keying) and M-QAM (M-ary quadrature amplitude modulation), which are widely employed in several communication systems [48]–[50].

This work aims to analyze the use of the fractional lower-order cyclic autocorrelation function (FLOCAF) and cyclic correntropy function (CCF) to obtain cyclic descriptors that allow the recognition of BPSK, QPSK, 8-QAM, 16-QAM, and 32-QAM modulations. Besides, a classification architecture based on such cyclic descriptors is also proposed for the robust classification of signals associated with the modulations mentioned above in scenarios with impulsive noise.

A. CONTRIBUTIONS
The main contributions, considering the scope of this work, can be outlined as follows:

- A mathematical demonstration is derived to show that the spatial sign cyclic correlation function (SSCCF) is a particular case of the FLOCAF;
- A detailed analysis about the cyclic spectrum of BPSK, QPSK, 8-QAM, 16-QAM, and 32-QAM signals obtained by the FLOCAF and CCF is provided, thus evidencing that such functions can extract singular descriptors capable of distinguishing the modulations above, even in environments contaminated by non-Gaussian alpha-stable noise;
- Automatic modulation classification architectures are proposed based on analysis of the cyclostationary signatures extracted by the FLOCAF and CCF;
- An exhaustive investigation on the parameters of the FLOCAF and CCF is presented in order to optimize their respective classification architectures;
- A performance comparison between the two proposed architectures in impulsive environments is provided;
- Numerical results are presented to demonstrate that it is possible to estimate the symbol rate parameter of the signals contaminated by non-Gaussian alpha-stable noise

from the cyclic descriptors obtained by the FLOCAF and CCF.

B. PAPER ORGANIZATION

This work is organized as follows: initially, Section II introduces the main concepts regarding alpha-stable distributions. Section III describes the main cyclostationary analysis functions, i.e., CAF, FLOCAF, and CCF. Section IV presents the spectral analysis of the functions mentioned above, applied to investigated modulations; moreover, the spectral analysis of the FLOCAF and CCF are extended to modulations contaminated with additive non-Gaussian alpha-stable noise. In Section V, the AMC architectures based on the FLOCAF and CCF are proposed, while Section VI presents the performance results of these architectures. In Section VII, a method to estimate the symbol rate parameter of the modulated signals, using the FLOCAF and CCF, is described. Finally, the main conclusions and further studies are presented in Section VIII.

II. ALPHA-STABLE DISTRIBUTIONS

Alpha-stable distributions may have Gaussian or non-Gaussian behavior. Non-Gaussian alpha-stable distributions have tails that can be modeled polynomially [51]. In other words, the farthest values from the center of the distribution will occur with a much higher probability in the non-Gaussian case than in the Gaussian one. Due to this heavy-tailed behavior, non-Gaussian alpha-stable distributions are commonly used in the modeling of channels subjected to impulsive noise of undetermined variance [26], [29], [52].

The fundamental principles associated with alpha-stable modeling are based on the generalized central limit theorem, which demonstrates that the sum of several independent and identically distributed (i.i.d.) random variables, with and without finite variance, converge to an alpha-stable distribution [34]. This behavior occurs due to the stability property, i.e., the linear combination of i.i.d. random variables whose distributions are alpha-stable result in another alpha-stable random variable [53].

Since the most distributions that belong to the alpha-stable family do not have a closed equation to define the probability density function, they are typically represented by the following characteristic function [53]:

$$\phi(\omega, \alpha, \beta, \gamma, \delta) = \exp\left\{\gamma^\alpha\left[-|\omega|^\alpha + j\omega\Theta(\omega, \alpha, \beta)\right] + j\delta\omega\right\}, \tag{1}$$

where:

$$\Theta(\omega, \alpha, \beta) = \begin{cases} \beta|\omega|^{\alpha-1}\tan\left(\dfrac{\pi\alpha}{2}\right) & \alpha \neq 1 \\ -\beta\dfrac{2}{\pi}\ln|\omega| & \alpha = 1, \end{cases} \tag{2}$$

being α the characteristic exponent or distribution stability index ($0 < \alpha \leq 2$). In non-Gaussian alpha-stable distributions ($\alpha < 2$), this parameter adjusts the impulsivity level of the density function. In turn, the parameter δ is responsible for adjusting the location of the distribution center.
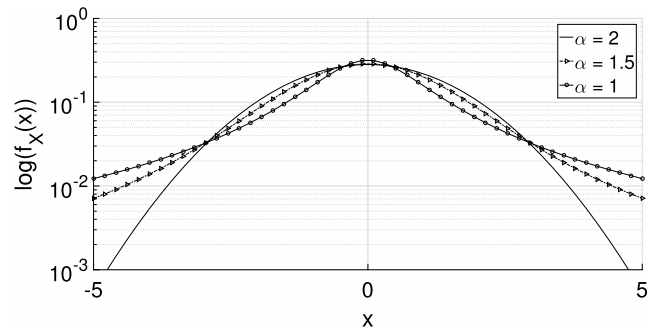
FIGURE 1. Probability density functions ($f_X(X)$) in logarithm scale for alpha-stable random variables (X) with different characteristic exponents and $\beta = 0, \gamma = 1, \delta = 0$. The lower the value of α, the slower the curve will decay and, therefore, the stronger the noise impulsivity will be.

The parameter γ is the dispersion or scaling parameter, whereas β adjusts the distribution symmetry ($-1 \leq \beta \leq 1$). If $\beta = 0$, the distribution is symmetric around its center; if $\beta > 0$, the distribution will be asymmetric to the right, whereas it is asymmetric to the left when $\beta < 0$. In the particular case where $\beta = 0$ and $\delta = 0$, the distributions are called symmetric alpha-stable [54].

Fig. 1 shows the relationship between the impulsivity in symmetric alpha-stable distributions and the tail heaviness in the logarithmic scale. The lower the value assumed by the characteristic exponent (α), the slower the tail will decay and, therefore, the stronger the noise impulsivity will be.

Non-Gaussian alpha-stable random variables only present finite statistical moments of order p when $0 \leq p < \alpha$. That is, for a non-Gaussian alpha-stable random variable X, the following properties are valid [55]:

$$E\left\{|X|^p\right\} = \infty, \quad \text{if } p \geq \alpha \tag{3}$$

and

$$E\left\{|X|^p\right\} < \infty, \quad \text{if } 0 \leq p < \alpha. \tag{4}$$

If $\alpha = 2$, then:

$$E\left\{|X|^p\right\} < \infty, \quad \text{for all } p \geq 0. \tag{5}$$

Therefore, alpha-stable distributions have no finite first- or higher-order moments for $0 < \alpha \leq 1$. Otherwise, if $1 < \alpha < 2$, they have the finite first-order moment and all the fractional moments of order $p < \alpha$. In this case, the parameter δ represents the mean value of the distribution. For $\alpha = 2$, all moments exist, and parameter γ is directly related to the distribution variance. In particular, all non-Gaussian alpha-stable distributions have infinite variance.

For some specific values of α, an alpha-stable distribution can be reduced to a simplified form that has a probability density function defined by an exact expression, such as the Gaussian[1] ($\alpha = 2$), Cauchy-Lorentz ($\alpha = 1$), and Lèvy distributions ($\alpha = 0.5$).

---

[1]Particularly, the alpha-stable distribution with ($\alpha = 2, \beta = 0, \gamma = \sigma/\sqrt{2}, \delta = \mu$) is reduced to the Gaussian form.

In channels that follow a non-Gaussian alpha-stable distribution, the signal-to-noise ratio (SNR) is not used as a channel quality indicator, since this measure will assume a value equal to zero. In this case, the geometric signal-to-noise ratio (GSNR) is usually employed as a quality indicator, which can be calculated as follows [56], [57]:

$$GSNR = \frac{A^2}{2\gamma^2 C_g^{\frac{2}{\alpha}-1}}, \tag{6}$$

where A is the root mean square (RMS) value of the transmitted signal; $C_g = e^{C_e} \approx 1.78$ is the exponential of the Euler constant, and $C_e \approx 0.5772$ is the Euler constant [33]. In the Gaussian case, the exponential of Euler constant ensures that the GSNR corresponds to SNR.

III. CYCLOSTATIONARY ANALYSIS
This section introduces the main statistical cyclostationary functions, namely the cyclic autocorrelation function, the fractional lower-order cyclic autocorrelation function, and the cyclic correntropy function. The concepts and mathematical basis of the functions are described in detail so that they can be appropriately compared with each other.

A. CYCLIC AUTOCORRELATION FUNCTION
A random process $x(t)$ is said cyclostationary in the wide sense when its mean value $E[x(t)]$ and its autocorrelation function $R_x(t, \tau)$ are both periodic in t within a period T for any value of τ [20], i.e.:

$$E\{x(t + T)\} = E\{x(t)\}, \tag{7}$$
$$R_x(t + T, \tau) = R_x(t, \tau), \tag{8}$$

where

$$R_x(t, \tau) = E\{x(t)x^*(t + \tau)\}. \tag{9}$$

Thus, in second-order cyclostationary processes, the autocorrelation function can be expanded in terms of the Fourier series as:

$$R_x(t, \tau) = \sum_\epsilon R_x^\epsilon(\tau)e^{j2\pi\epsilon t}, \tag{10}$$

where $R_x^\epsilon(\tau)$ represents the Fourier series coefficients given by:

$$R_x^\epsilon(\tau) \triangleq \frac{1}{T} \int_{-T/2}^{T/2} R_x(t, \tau)e^{-j2\pi\epsilon t} dt. \tag{11}$$

Such coefficients define the cyclic autocorrelation function (CAF), where ϵ is a discrete parameter hereafter called cyclic frequency ($\epsilon = n/T, \forall n \in Z$). The CAF can be interpreted as an analytic function that verifies if the process $x(t)$ is cyclostationary by evaluating if $R_x^\epsilon(\tau)$ is non-null for at least a $\epsilon \neq 0$. In turn, when $R_x(t, \tau)$ has multiple fundamental frequencies, then $x(t)$ is said to be a polycyclostationary process [19]. In this case, the CAF can be expressed by [19]:

$$R_x^\epsilon(\tau) \triangleq \lim_{T \to \infty} \frac{1}{T} \int_{-T/2}^{T/2} R_x(t, \tau)e^{-j2\pi\epsilon t} dt. \tag{12}$$
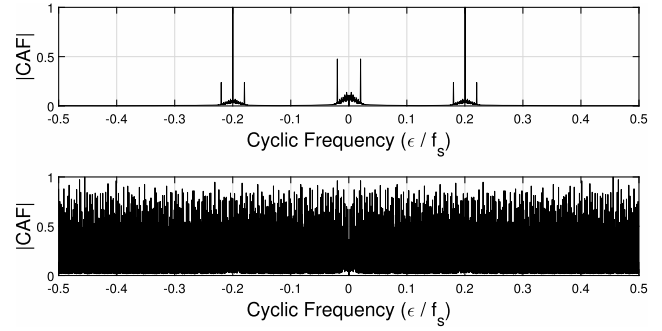
FIGURE 2. Second-order cyclic autocorrelation function applied to BPSK signal without and with alpha-stable contamination. When contamination exists, it is not possible extract second-order cyclostationary features.

Although the second-order cyclostationary analysis has several applications, it is not suitable for non-Gaussian alpha-stable process [21], since they have an unlimited second-order moment. This aspect can be observed in Fig. 2, which shows two cyclostationary signatures of a BPSK signal, being the first one without contamination and the second one contaminated by symmetrical and centralized alpha-stable additive noise with $GSNR = 15$ dB and $\alpha = 1.5$. When the BPSK signal is contaminated by non-Gaussian alpha-stable noise of infinite variance, it is not possible to obtain the second-order cyclostationary features.

B. FRACTIONAL LOWER-ORDER CYCLIC AUTOCORRELATION FUNCTION
Since signals contaminated by additive non-Gaussian alpha-stable noise cannot be analyzed for statistical moments of order $p \geq 2$, the statistical characterization of such signals can be achieved by using lower-order statistical moments, particularly the fractional lower-order covariance (FLOC), which can be defined as [45]:

$$R_x^{a,b}(t, \tau) = E\left\{\left[x(t)|x(t)|^{(a-1)}\right] \times \left[x^*(t+\tau)|x^*(t+\tau)|^{(b-1)}\right]\right\}, \tag{13}$$

where a and b are the fractional lower-order parameters of $R_x^{a,b}(t, \tau)$. Unlike second-order moments, FLOC is finite when applied to symmetric alpha-stable distributions whenever the following inequality is valid:

$$0 \leq a, b < \alpha/2. \tag{14}$$

When incorporated into the cyclostationary analysis, FLOC gives rise to the fractional lower-order cyclic autocorrelation function (FLOCAF), which is defined as [45]:

$$R_x^{\epsilon,ab}(\tau) \triangleq \frac{1}{T} \int_{-T/2}^{T/2} R_x^{a,b}(t, \tau)e^{-j2\pi\epsilon t} dt. \tag{15}$$

In this case, the FLOCAF makes it possible to verify if a given process $x(t)$ is cyclostationary, even when contaminated by infinite variance noise by evaluating if $R_x^{\epsilon,ab}(\tau)$ is non-null for any $\epsilon \neq 0$.

An interesting aspect of the FLOCAF can be seen when its parameters of lower-order statistical moments (a, b) are zero.

In this case, FLOC can be represented as follows:

$$R_x^{0,0}(t, \tau) = E \left\{ \frac{x(t)}{|x(t)|} \times \frac{x^*(t + \tau)}{|x^*(t + \tau)|} \right\}. \tag{16}$$

However, in order to avoid discontinuity when $x(t)$ and $x(t + \tau)$ are equal to zero, $R_x^{0,0}$ must be represented in terms of the spatial sign function [41], [58] defined by:

$$S(x(t)) = \begin{cases} \dfrac{x(t)}{|x(t)|} & x(t) \neq 0 \\ 0 & x(t) = 0. \end{cases} \tag{17}$$

Therefore, (16) can be rewritten as:

$$R_x^{0,0}(t, \tau) = E \left\{ S(x(t)) \, S\left(x^*(t + \tau)\right) \right\}. \tag{18}$$

Applying $R_x^{0,0}(t, \tau)$ to FLOCAF and assuming that $x(t)$ is a polycyclostationary process gives:

$$R_x^{\epsilon,00}(\tau) = \lim_{T \to \infty} \frac{1}{T} \int_{-T/2}^{T/2} E \left\{ S(x(t)) S(x^*(t + \tau)) \right\} e^{-j2\pi\epsilon t} \, dt, \tag{19}$$

and considering that $R_x^{\epsilon,00}(\tau)$ is polycycloergodic, it is possible to rewrite (19) as:

$$R_x^{\epsilon,00}(\tau) \triangleq \lim_{T \to \infty} \frac{1}{T} \int_{-T/2}^{T/2} S(x(t)) S(x^*(t + \tau)) e^{-j2\pi\epsilon t} \, dt. \tag{20}$$

Equation (20) is also known as the spatial sign cyclic correlation function (SSCCF), being denoted by $R_S(\epsilon, \tau)$ [41], [43].

Thus, the SSCCF can be seen as a particular case of FLOCAF if the parameters a and b of the latter function are both equal to zero. The SSCCF will always converge when applied to alpha-stable distributions, independent of the characteristic exponent (α) because it will always meet the condition established in (14). In other words, this function is more robust to the presence of impulsive noise than any other FLOCAF configuration. However, there is no guarantee that the SSCCF returns the best cyclic descriptors of a signal when considering all other FLOCAF settings in terms of a and b.

C. CYCLIC CORRENTROPY FUNCTION

Another approach for the analysis of cyclostationary features of signals contaminated with additive non-Gaussian alpha-stable noise can be defined when using the cyclic correntropy function (CCF). The CCF is based on the correntropy function, which is a nonlinear transformation defined by [39]:

$$V_x(t, \tau) = E \left\{ k_\sigma(x(t) - x(t + \tau)) \right\}, \tag{21}$$

where $k_\sigma(\cdot)$ is any unimodal, symmetric, and positive definite function, denominated kernel. In this work, a Gaussian kernel is employed, which is defined by [21]:

$$G_\sigma\left(x(t), x(t + \tau)\right) = \frac{1}{\sigma\sqrt{2\pi}} \exp\left(-\frac{[x(t) - x(t + \tau)]^2}{2\sigma^2}\right), \tag{22}$$

where σ is the kernel size. Thus, it is possible to rewrite (21) as:

$$V_x(t, \tau) = E \left\{ G_\sigma(x(t), x(t + \tau)) \right\}. \tag{23}$$

Let us assume that the correntropy function is periodic in t with period T, i.e.,

$$V_x(t + T, \tau) = V_x(t, \tau). \tag{24}$$

Therefore, it can be expanded in the form of a Fourier series as follows:

$$V_x(t, \tau) = \sum_{\epsilon} V_x^{\epsilon}(\tau) e^{j2\pi\epsilon t}, \tag{25}$$

where $V_x^{\epsilon}(\tau)$ represents the series coefficients, given by:

$$V_x^{\epsilon}(\tau) = \frac{1}{T} \int_{-T/2}^{T/2} V_x(t, \tau) e^{-j2\pi\epsilon t} \, dt, \tag{26}$$

which defines the CCF.

Analogously to the CAF, parameter ϵ represents the cyclic frequencies ($\epsilon = n/T, \forall n \in Z$). When $V_x(t, \tau)$ has multiple fundamental frequencies, then $x(t)$ is said to be a polycyclostationary process [21]. In this case, the CCF can be defined as:

$$V_x^{\epsilon}(\tau) \triangleq \lim_{T \to \infty} \frac{1}{T} \int_{-T/2}^{T/2} V_x(t, \tau) e^{-j2\pi\epsilon t} \, dt. \tag{27}$$

Using the Gaussian kernel $G_\sigma(\cdot, \cdot)$ for the calculation of the cyclic correntropy and considering operator $\langle \cdot \rangle$, defined by:

$$\langle \cdot \rangle = \lim_{T \to \infty} \frac{1}{2T} \int_{-T}^{T} (\cdot) \, dt, \tag{28}$$

then (27) can be rewritten as:

$$V_x^{\epsilon}(\tau) = \left\langle E\{G_\sigma(x(t), x(t + \tau))\} e^{-j2\pi\epsilon t} \right\rangle. \tag{29}$$

Assuming that $V_x^{\epsilon}(\tau)$ is polycycloergodic [19], [21], it is possible to represent (29) as [21]:

$$V_x^{\epsilon}(\tau) = \left\langle G_\sigma(x(t), x(t + \tau)) e^{-j2\pi\epsilon t} \right\rangle$$
$$= \left\langle \frac{1}{\sqrt{2\pi}\sigma} \exp\left(\frac{-[x(t) - x(t + \tau)]^2 - 2\sigma^2 j2\pi\epsilon t}{2\sigma^2}\right) \right\rangle. \tag{30}$$

Due to the Gaussian kernel exponential decay in (30), the cyclic correntropy function will always converge, even when calculated over a process $x(t)$ subjected to an additive impulsive noise modeled by a non-Gaussian alpha-stable process. This issue ensures robustness of the function to outliers generated by impulsive noise channels, which have less influence on $V_x^{\epsilon}(\tau)$ since they are further from the Gaussian kernel center. Another interesting feature addressed

to the CCF can be observed while expanding (29) into a Maclaurin series:

$$V_x^\epsilon(\tau) = \frac{1}{\sigma\sqrt{2\pi}} \left\langle \sum_{n=0}^{\infty} \frac{(-1)^n}{(2\sigma^2)^n n!} E\{[(x(t) - x(t+\tau))^2 + 2\sigma^2 2j\pi\epsilon t]^n\} \right\rangle. \quad (31)$$

From (31), it can be stated that $V_x^\epsilon(\tau)$ contains infinite statistical moments information associated with the second-order one, which are strongly related to the kernel size (σ). Larger kernel sizes will contribute to lower-order statistical moments, with a greater influence of such moments on the calculation of the CCF. On the other hand, smaller ones will make the high-order moments more relevant in the calculation of $V_x^\epsilon(\tau)$.

Due to such characteristics, the cyclic correntropy may be able to extract higher-order statistical information from cyclostationary processes that cannot be typically analyzed by the CAF, since the latter function performs a second-order analysis.

IV. CYCLIC SPECTRAL ANALYSIS

In this section, the cyclic spectral analysis of BPSK, QPSK, 8-QAM, 16-QAM, and, 32-QAM modulations, is provided. First, a comparison among cyclostationary signatures obtained by the CAF, FLOCAF, and, CCF, without noise contamination, is presented. Then, an examination of the FLOCAF and CCF signatures, on the alpha-stable channel, is discussed.

A. CAF VERSUS FLOCAF VERSUS CCF WITHOUT CONTAMINATION

As treated in the previous section, since the FLOCAF and CCF converge, even under contamination of noise with infinite variance, both functions can provide cyclostationary signatures robust to impulsive noise contamination. However, a detailed spectral analysis of the cyclostationary signatures for digital modulations, using the functions mentioned above, has not yet been performed in the literature, particularly in the case of M-PSK and M-QAM.

Therefore, this section provides an investigation of the ability from the FLOCAF and CCF to extract singular cyclostationary features from modulations BPSK, QPSK, 8-QAM, 16-QAM, and, 32-QAM, provided by the FLOCAF and CCF. For a comprehensive comparative analysis, the cyclostationary signatures produced by the CAF is also evaluated.

The functions are applied to modulated signals with the same intermediate frequency f_i, symbol rate f_b, and sampling frequency f_s to extract the signatures. The cyclic frequency at $\epsilon = 0$ was suppressed in all obtained signatures since it is a common parameter. Besides, this central component is the one that carries the most amount of energy, being responsible for hiding the other cyclic frequencies components. The cyclostationary features extracted by each function when applied to noiseless signals are represented in Fig. 3 to Fig. 7.
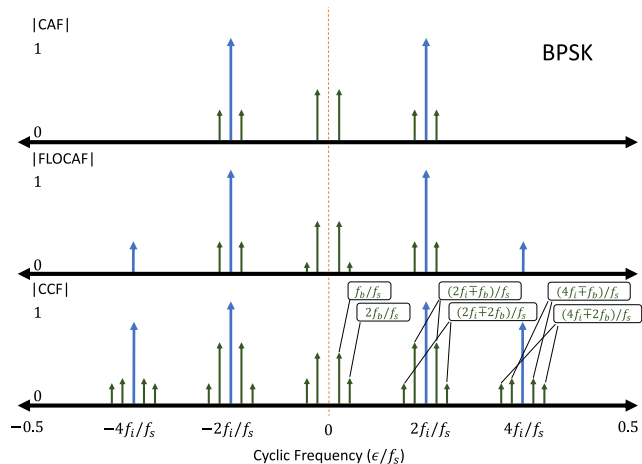

FIGURE 3. BPSK cyclostationary signatures obtained by the CAF, FLOCAF, and CCF.
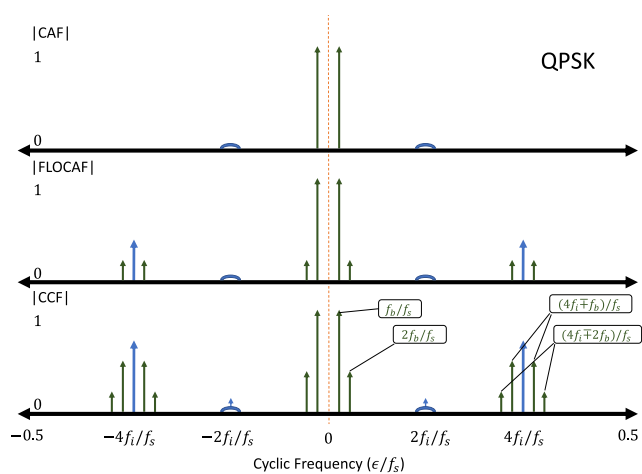

FIGURE 4. QPSK cyclostationary signatures obtained by the CAF, FLOCAF, and CCF.

Fig. 3 shows the BPSK cyclostationary signatures generated respectively by the CAF, FLOCAF, and CCF. The signature generated by FLOCAF contains all the cyclic descriptors that exist in the CAF signature, but additional cyclic components at $\pm 2f_b/f_s$ and $\pm 4f_i/f_s$ are evidenced in this case. In turn, a signature generated by the CCF contains all the cyclic components provided by FLOCAF, among which some of them present higher amplitudes, while new cyclic components are presented at $(2f_i \pm 2f_b)/f_s$, $(4f_i \pm f_b)/f_s$ and $(4f_i \pm 2f_b)/f_s$.

Fig. 4 shows the cyclostationary signatures associated with the QPSK modulation. In this case, the signature generated by FLOCAF aggregates all cyclic components provided in the CAF signature, and also cyclic components at $\pm 2f_b/f_s$, $\pm 4f_i/f_s$ and $\pm(4f_i \pm f_b)/f_s$. On the other hand, the signature generated by the CCF presents all the cyclic components regarding FLOCAF signature, and also new ones at $\pm(2f_i \pm 2f_b)/f_s$ and $\pm(4f_i \pm 2f_b)/f_s$.

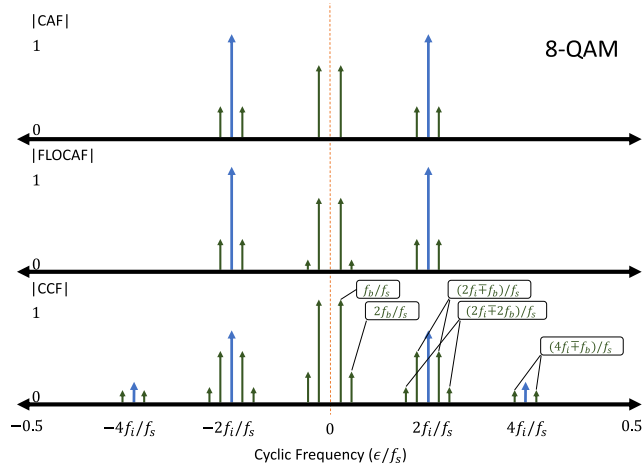The results in Fig. 5 to Fig. 7 show that the cyclostationary signatures of the 8-, 16- and 32-QAM modulations have

FIGURE 5. 8-QAM cyclostationary signatures obtained by the CAF, FLOCAF, and CCF.
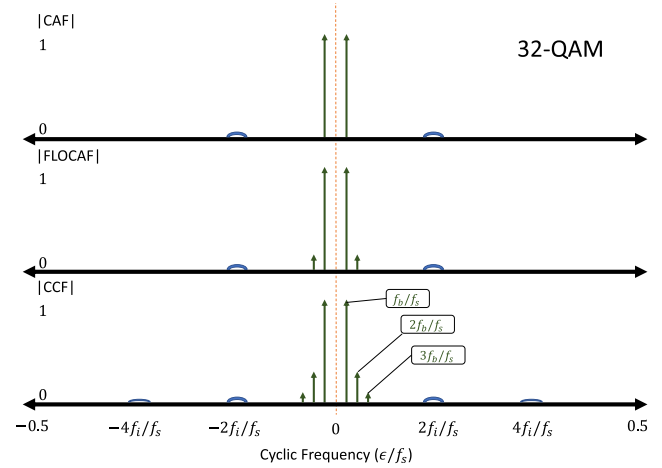

FIGURE 7. 32-QAM cyclostationary signatures obtained by the CAF, FLOCAF, and CCF.
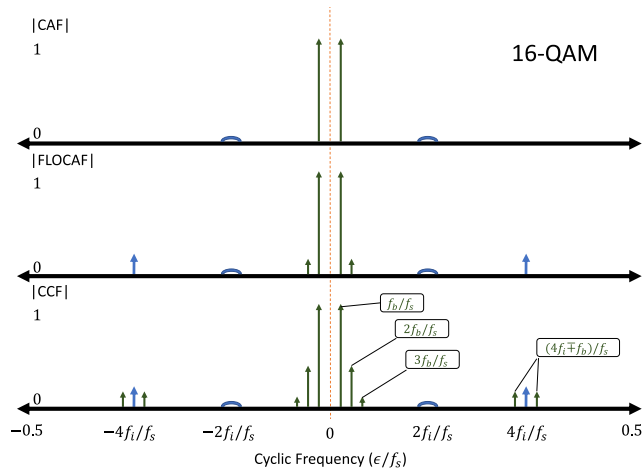

FIGURE 6. 16-QAM cyclostationary signatures obtained by the CAF, FLOCAF, and CCF.

similar behavior to those previously described for the BPSK and QPSK modulations. In all cases, the signatures provided by FLOCAF contain all cyclic components presented by the signatures generated by CAF, while also introducing new descriptors. Similarly, the CCF signatures contain all the cyclic components regarding FLOCAF and also present new components in the respective cyclic spectrum.

The signatures generated by CAF shows that it is not effective in extracting cyclic information capable of characterizing, properly, each modulation. The cyclic signatures associated with BPSK and 8-QAM shown in Fig. 3 and Fig. 5, respectively, have the same profile. This aspect can also be seen at QPSK, 16-QAM, and 32-QAM, which have identical signatures.

On the other hand, the FLOCAF is capable of extracting singular descriptors for each modulation technique, although the signatures regarding 16-QAM and 32-QAM present slight differences as shown in Fig. 6 and Fig. 7, respectively.

The CCF is also able to extract unique signatures for each modulation. The obtained signatures contain all

components presented by the FLOCAF, and also additional cyclic frequency ones. In this case, the signatures obtained with the CCF present some differences between 16-QAM and 32-QAM.

Moreover, all the cyclic components presented in the signatures generated by the CCF are directly related to the intermediate frequency (f_i) and symbol rate (f_b) of the analyzed signals. Thus, in addition to robustness to impulsive noise [21], [45], the FLOCAF and CCF are capable of extracting unique signatures from BPSK, QPSK, 8-QAM, 16-QAM, and 32-QAM.

B. FLOCAF VERSUS CCF ON ALPHA-STABLE CHANNEL

The performances of the FLOCAF and CCF for obtaining cyclostationary features from digital modulations, in impulsive environments, are discussed in this section. For that, an analysis with BPSK, QPSK, 8-QAM, 16-QAM, and, 32-QAM signals contaminated by additive symmetric alpha-stable noise, is provided. The contaminated signal can be expressed as:

$$x(t) = s(t) + n(t), \qquad (32)$$

where, $n(t)$ is the α-stable noise and

$$s(t) = A(t)cos(2\pi f_i + \theta(t)). \qquad (33)$$

The term $A(t)$ is the amplitude of the signal, f_i represents an intermediate frequency, and $\theta(t)$ is the signal phase. All these parameters are defined according to the modulation format adopted for information transmission.

Table 1 presents the sampling frequency, intermediate frequency, and symbol rate employed in the generation of the modulated signals, besides the parameters regarding the CCF and FLOCAF setting. The channel was modeled as an alpha-stable distribution with the following parameters: characteristic exponent $\alpha = 1.5^2$, symmetry $\beta = 0$, location $\delta = 0$,

---

[2]This value of characteristic exponent was adopted to define a distribution fairly impulsive [45], [59]

TABLE 1. Simulation parameters.

Parameter	Value
Sampling frequency (f_s)	10 kHz
Intermediate frequency (f_i)	1 kHz
Symbol rate (f_b)	200 baud
Fractional lower-order	$a = 0.3, b = 0.5$
Kernel size	$\sigma = 1.1$
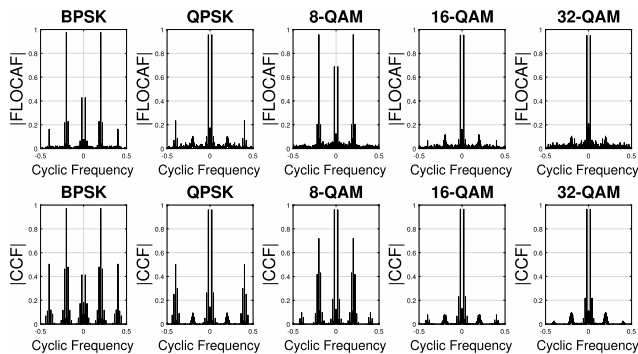
FIGURE 8. Fractional lower-order cyclic autocorrelation function versus cyclic correntropy function (GSNR = 10 dB).
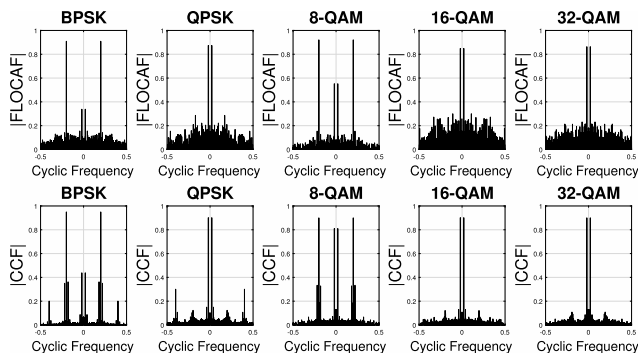
FIGURE 9. Fractional lower-order cyclic autocorrelation function versus cyclic correntropy function (GSNR = 0 dB).

and GSNR equal to 10 dB, and 0 dB. The cyclostationary signatures obtained are shown in Fig. 8 and Fig. 9.

Fig. 8 compares the signatures of the modulations generated by the FLOCAF and CCF considering an alpha-stable additive noise contamination with GSNR = 10 dB. In both cases, the functions can obtain unique signatures for each one of the modulations, since the specific positions and amplitudes of the cyclic components are not the same.

Fig. 9 represents the cyclostationary signatures for signals contaminated by alpha-stable noise with GSNR = 0 dB obtained by the FLOCAF and CCF. The comparing of both figures above shows that, as the impulsive noise contamination grows, the degradation of the cyclostationary signatures increases.

In this context, the signatures generated by FLOCAF are very sensitive to noise contamination. In other words, the cyclic frequency components, of some signatures, when in low GSNR condition, are significantly attenuated and even faded, resulting in difficulty to distinguish among modulation signatures, e.g., QPSK, 16-QAM, and 32-QAM.

On the other hand, the signatures generated by the CCF present enough cyclostationary information to allow distinguishing the modulations accurately, with less difference between 16-QAM and 32-QAM.

Since the signatures, provided by the FLOCAF and CCF, presents dynamic behaviors for the variation of GSNR conditions, a more accurate comparing of both functions is provided applying them to automatic modulation classification architectures.

Therefore, in Section V, AMC architectures, based on the FLOCAF and CCF, are proposed, and in Section VI the performances of both architectures are compared.

V. AUTOMATIC MODULATION CLASSIFICATION ARCHITECTURES

As previously demonstrated, the FLOCAF and CCF can extract singular cyclostationary descriptors for each analyzed modulation even in impulsive noise environments. This section describes the AMC architectures based on the functions mentioned above. The schematic diagram of the architectures is depicted in Fig . 10.

A. DEFINITION OF MODULATION TEMPLATES

The architectures perform a comparison between the cyclic profiles of the input signal and the cyclic profiles of the noiseless modulation signals available for classification, which will be called hereafter by templates. The main difference between the architectures is the cyclostationary function used in the calculation of cyclic profiles. The FLOCAF-based architecture uses FLOCAF to generate the templates and the cyclic profile of the input signal. The same approach specifies CCF-based architecture.

B. UNKNOWN SIGNAL

The cyclic profile of the unknown input signal must be generated following the same processes used in the templates. Thus, if the architecture uses FLOCAF, the fractional lower-order moments (*a* and *b*) that configure the function must be the same for both: the templates and the input signal cyclic profile. Similarly, if the architecture uses the CCF, both the templates and the signature of the input signal must be parameterized with the same kernel size (σ).

C. CORRELATION COEFFICIENT

The second step of the proposed architectures is to compare the unknown signal with the templates. For this, the similarity measure, known as the Pearson correlation coefficient, is adopted in this work, which is given by:

$$\rho = \frac{COV(X, Y)}{\sqrt{VAR(X)VAR(Y)}}. \tag{34}$$

Pearson's correlation coefficient is a technique of low computational complexity that returns values ranging from -1 to 1, which can be classified as follows: $|\rho| < 0.3$ denotes uncorrelated elements; $0.3 \leq |\rho| \leq 0.5$ denotes poor correlation; $0.5 < |\rho| \leq 0.7$ denotes moderate correlation;
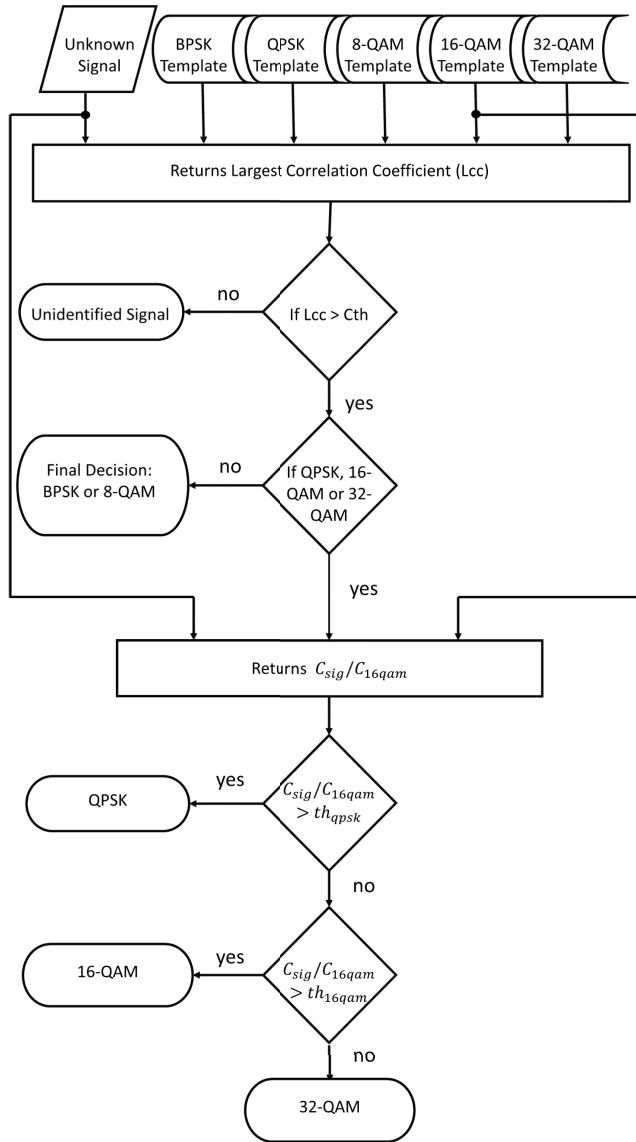
FIGURE 10. AMC Architecture based on cyclostationary feature extraction.

$0.7 < |\rho| \le 0.9$ indicates strong correlation; $|\rho| > 0.9$ indicates very strong correlation[3] [60].

In the proposed architectures, the cyclostationary signature of the input signal is correlated with all the templates, where the largest coefficient (L_{CC}) value among them is used to classification. The chosen coefficient is compared with a previously defined correlation threshold (C_{th}). If the largest correlation coefficient is lower than C_{th}, the input signal will not be recognized.

This action contributes to reducing the false-positive problem, that occurs when the predicted modulation is improperly indicated. In other words, the correlation criterion supports the correct modulation classification, helping to reduce the biased decision for a specific class.

[3]In fact, the Pearson correlation coefficient when negative is said to be inversely correlated.

The incidence of false-positives decreases as higher the threshold; however, an elevated threshold also contributes to decreasing of true-positives classification, which results in a decrease of classifier hit-rate. Therefore, to establish a suitable hit-rate adjust, and limit the false-positive occurrences, the chosen threshold was $C_{th} = 0.7$, since this value guarantees moderate to strong correlation.

In case $L_{CC} > C_{th}$, the decision of the input signal class is made. When the L_{CC} is associated with the BPSK or 8-QAM template, the predicted modulation is respectively attributed to BPSK or 8-QAM class. Otherwise, the architectures will follow other steps to distinguish QPSK, 16-QAM, and, 32-QAM.

D. C_{SIG}/C_{16QAM} RATIO

According to Fig. 6 and Fig. 7, the cyclostationary signatures of 16-QAM and 32-QAM, generated by the FLOCAF and CCF, have few differences. Among them, the most evident one is the cyclic component at the spectral position $4f_i$ that appears in the signatures associated with the 16-QAM, while it is absent in the 32-QAM. Besides that, Fig. 4 shows that the element at the spectral position $4f_i$, in the QPSK signature, is also the principal difference between that modulation and 16-QAM, whereas this component in the QPSK signature is more significant than in the 16-QAM signature.

This way, to classify the input signal among QPSK, 16-QAM, and, 32-QAM, was used the ratio between its cyclic component at position $4f_i$ (C_{sig}) and the component of the template of 16-QAM (C_{16QAM}) at the same spectral position $4f_i$. The criterion applied to choose the class in which the signal belongs consists of comparing the relation C_{sig}/C_{16QAM} with two thresholds, the QPSK threshold (th_{QPSK}) and the 16-QAM threshold (th_{16QAM}).

In case that $C_{sig}/C_{16QAM} > th_{QPSK}$, the input signal will be attributed to the QPSK class. When $th_{QPSK} > C_{sig}/C_{16QAM} > th_{16QAM}$, the input signal will be classify as 16-QAM. Otherwise, if $th_{16QAM} > C_{sig}/C_{16QAM}$, the choose class will be 32-QAM. The thresholds are defined based on an extensive investigation of C_{sig}/C_{16QAM} ratio, in a specific GSNR condition. This process is more detailed in the next section.

VI. AMC EXPERIMENTS

In this section, the performances of the classification architectures based on the cyclostationary features, obtained by the FLOCAF and CCF, are evaluated in impulsive environments.

The environments were characterized by a non-Gaussian additive alpha-stable noise with the following parameters: characteristic exponent $\alpha = 1.5$, symmetry $\beta = 0$, location $\delta = 0$, and GSNR ranging from -10 dB to 10 dB with the step of 2 dB. The modulated signal parameters, i.e., sampling frequency, intermediate frequency, and symbol rate, are the same defined in Table 1 from Section IV-B.

A. AMC USING THE FLOCAF

In the FLOCAF-based AMC architecture test, an extensive search is performed to determine the fractional
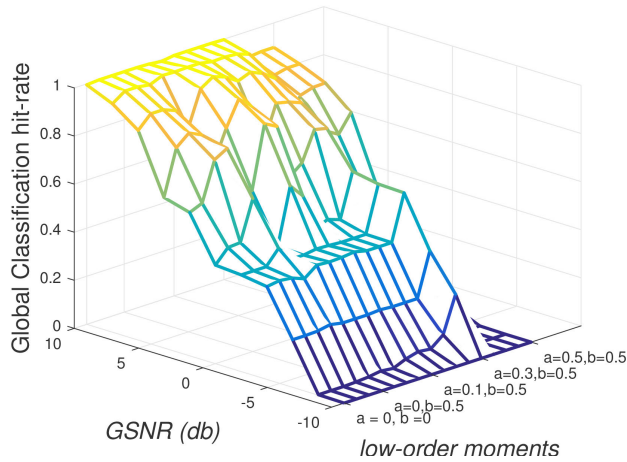
FIGURE 11. Global automatic modulation classification using the FLOCAF for different kernel sizes, after calculating the average of GSNR.

FIGURE 12. Average Global classification hit-rate for the considered GSNR range, for distinct fractional lower-order moments, obtained by the FLOCAF-based architecture.

lower-order parameters (i.e., a and b) that allow optimizing its performance. Thus, the architecture was parameterized for all combinations of a and b assuming the following values: {0; 0.1; 0.3; 0.5}, which are chosen to meet the convergence criterion represented in (14).

The architecture was tested as follows: first, the noisy input signals, which can assume any of the proposed modulations, were generated several times for each value of GSNR and applied to the architecture. Then, the global classification rate, which is the average among the classification rates of each modulation, was calculated considering 100 iterations per modulation, for each value of GSNR. Finally, different classification curves were obtained, changing the fractional lower-order parameters and varying the GSNR.

Fig. 11 shows that the FLOCAF-based architecture has distinct behavior, in terms of hit-rate, for each combination of a and b, which also varies with the GSNR. Therefore, to determine the fractional lower-order parameters that optimize the architecture performance for a medium-quality channel in terms of the GSNR, an average hit-rate was calculated considering the GSNR ranging from -10 dB to 10 dB. The result is shown in Fig. 12.

In the particular case when $a = b = 0$, FLOCAF becomes the SSCCF, and therefore, the cyclostationary descriptors will be less affected by impulsive noise. However, the results in Fig. 12 demonstrate that, on average, the architecture can correctly classify more modulation types when parameterized with $a = 0.3$ and $b = 0.5$. This result suggests that the digital modulations evaluated contain cyclostationary information that is better evidenced by such specific fractional lower-order parameters.

After determining the cyclic function parameters that optimize the average performance of the architecture, a more detailed analysis of the classifier can be performed, considering 1,000 iterations per modulation, for each value of the GSNR.

The th_{QPSK} and th_{16QAM} were defined considering a comprehensive analysis of signatures of QPSK, 16-QAM, and,
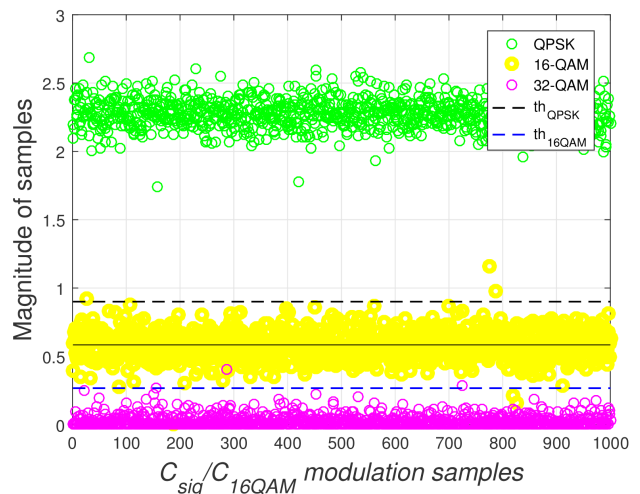
FIGURE 13. Definition of th_{qpsk} and th_{16QAM} thresholds.

32-QAM modulations, under the noise contamination corresponding to $GSNR = 10$ dB. For that, each modulation signature was generated 1, 000 times, and the factor C_{sig}/C_{16QAM} was calculated for each one of them.

The analysis, presented in Fig. 13, shows that the samples associated with 16-QAM are in a particular range of magnitude that is between QPSK and 32-QAM ranges. Therefore, the th_{qpsk} and th_{16QAM} were respectively established considering three standard deviations above, and three standard deviations below the mean value of 16-QAM samples. The adopted thresholds in the FLOCAF-based AMC architecture, are presented in Table 2.

After setting the fractional lower-orders parameters (a and b), and adjusting of the thresholds, the architecture was tested, and its classification behavior is shown in Fig. 14.

Fig. 14 shows that the architecture based on FLOCAF has a distinct classification performance for each modulation. The classification hit-rates achieves values above of 90% in the GSNR = 0 dB, for BPSK, 8-QAM, and, 32-QAM

TABLE 2. Thresholds of FLOCAF-based AMC architecture.

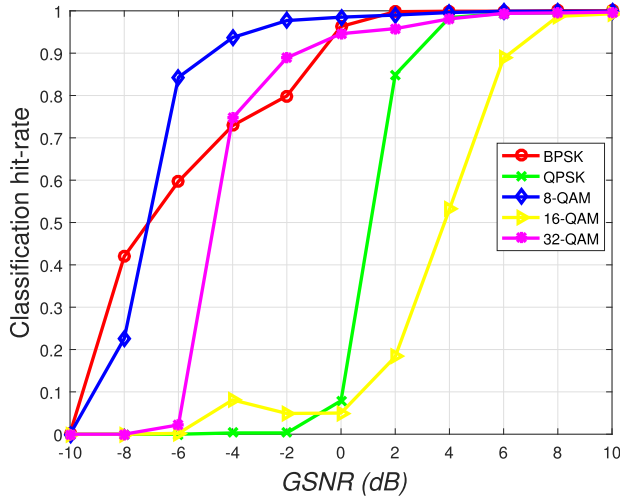| Parameter	Value
C_{th}	0.70
th_{QPSK}	0.90
th_{16QAM}	0.26

FIGURE 14. Modulation classification curves of FLOCAF-based architecture with $a = 0.3$ and $b = 0.5$, and 1,000 interactions per GSNR.

TABLE 3. Confusion Matrix of FLOCAF ($a = 0.3$, $b = 0.5$, GSNR = 0 dB).

Modulation Classification	Actual Modulation				
	BPSK	QPSK	8QAM	16QAM	32QAM
BPSK	963	0	0	0	0
QPSK	0	79	0	0	0
8QAM	31	0	985	0	0
16QAM	0	869	0	50	15
32QAM	0	4	0	919	946
Below C_{th}	6	48	15	31	39

modulations. While for QPSK modulation, the architecture needs GSNR = 4 dB.

When GSNR = 8 dB, the architecture achieves a hit-rate close to 100% for all modulations. Since the classifier presents a particular behavior in each GSNR condition, for more detailed analysis, the confusion matrices of some GSNR instances are given in Tables 3 to 5.

The summarized results show that, for low GSNR levels, the QPSK modulation is widely confused with 16-QAM. Thus, it is inferred that for a very high noise level, some cyclic components from QPSK modulation are attenuated resulting in a signature that is more approximate of the 16-QAM template than of the QPSK template. However, the matrices also indicate that, as the GSNR increases, the accuracy of QPSK classification grows.

Similar behavior occurs for the 16-QAM classification, for low GSNR levels, this modulation is widely confused with 32-QAM. Just as in the case discussed above, as the GSNR increases, the accuracy of the 16-QAM classification also increases. However, the hit-rate of this modulation growing

TABLE 4. Confusion Matrix of FLOCAF ($a = 0.3$, $b = 0.5$, GSNR = 4 dB).

Modulation Classification	Actual Modulation				
	BPSK	QPSK	8QAM	16QAM	32QAM
BPSK	999	0	0	0	0
QPSK	0	984	0	0	0
8QAM	0	0	996	0	0
16QAM	0	0	0	531	5
32QAM	0	0	0	451	981
Below C_{th}	1	16	4	18	14

TABLE 5. Confusion Matrix of FLOCAF ($a = 0.3$, $b = 0.5$, GSNR = 10 dB).

Modulation Classification	Actual Modulation				
	BPSK	QPSK	8QAM	16QAM	32QAM
BPSK	1000	0	0	0	0
QPSK	0	998	0	2	0
8QAM	0	0	999	0	0
16QAM	0	0	0	993	3
32QAM	0	0	0	2	997
Below C_{th}	0	2	1	3	0

slower, which indicates that 16-QAM is more sensitive to noise contamination than other analyzed modulations.

These results also indicate that, for the classification criteria adopted in the proposed architecture, the cyclic signatures of BPSK, 8-QAM, and, 32-QAM are the most robust to impulsive noise contamination, once that, even for some negative GSNR values, the classification hit-rates for these modulations are elevated.

B. AMC USING CCF

In the test of the CCF-based AMC architecture, analogously to the case of FLOCAF, an extensive search is performed to determine the best kernel size (σ) that allows optimizing the overall performance. In this case, all values in the range from 0.1 to 1.4 with steps of 0.1 were evaluated.

The experiment was conducted as follows: first, the noisy input signal, which may assume one of the modulations, was generated several times for each GSNR condition and applied to the architecture. Then, the global classification rate was calculated, considering 100 iterations per modulation, for each value of GSNR. Finally, different classification curves were obtained for each modulation considering the GSNR variation. The results are represented in Fig. 15.
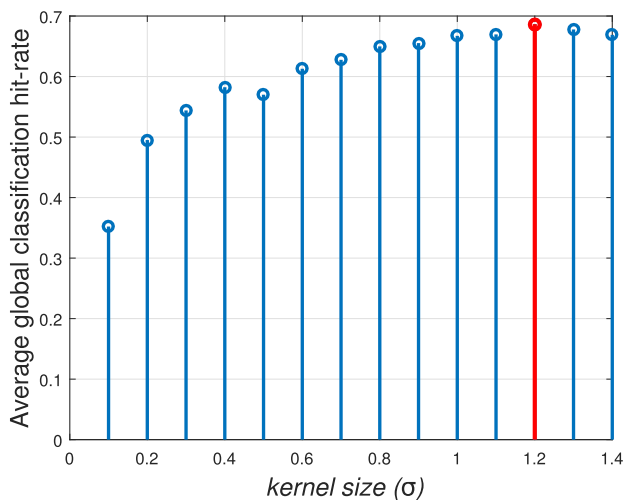
Fig. 15 shows that the CCF-based AMC architecture has distinct behavior, in terms of hit-rate, for each kernel size, which also varies with the GSNR. Therefore, to determine the value that optimizes the architecture performance for a medium-quality channel, the average of global hit-rate related to the GSNR range was verified.

The results in Fig. 16 denote that, on average, the architecture achieved the highest hit-rate when parameterized with $\sigma = 1.2$. Thus, after finding the best kernel size for the investigated configurations, more detailed classifier tests, considering 1,000 iterations per modulation, for each GSNR value, can be performed.

The th_{QPSK} and th_{16QAM} were defined considering an analysis of signatures of QPSK, 16-QAM, and, 32-QAM in
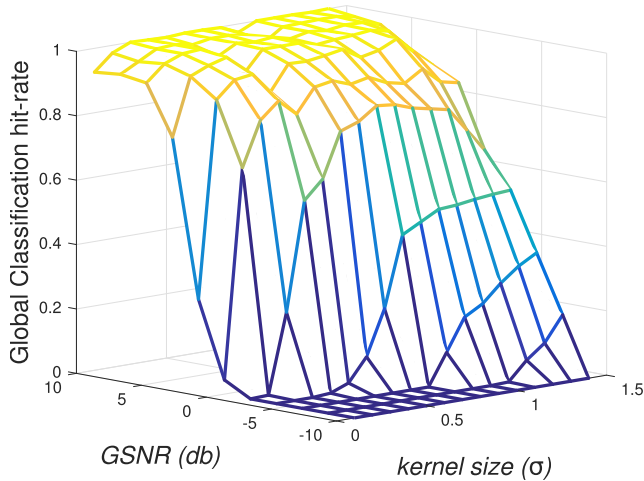
FIGURE 15. Global classification hit-rate using the CCF for different kernel sizes, with 100 interactions while varying the GSNR.

FIGURE 16. Global automatic modulation classification using the CCF for different kernel sizes, after calculating the average of GSNR.

TABLE 6. Thresholds of CCF-based AMC architecture.

| Parameter	Value
C_{th}	0.70
th_{QPSK}	1.29
th_{16QAM}	0.52

an α-stable channel with $GSNR = 10$ dB. Modulation signatures were generated $1,000$ times, and the factor C_{sig}/C_{16QAM} was calculated for each one of them.

Fig. 17, shows that the samples associated with 16-QAM are in a particular range of magnitude that is between QPSK and 32-QAM ranges. This way, as in the case of the FLOCAF-based architecture, the th_{qpsk} and th_{16QAM} were established considering three standard deviations above, and three standard deviations below the mean value of 16-QAM samples. The adopted thresholds in the CCF-based AMC architecture are presented in Table 6.

After setting the kernel size (σ), and adjusting of the thresholds, the CCF-based architecture was tested, and its classification behavior is shown in Fig. 18.
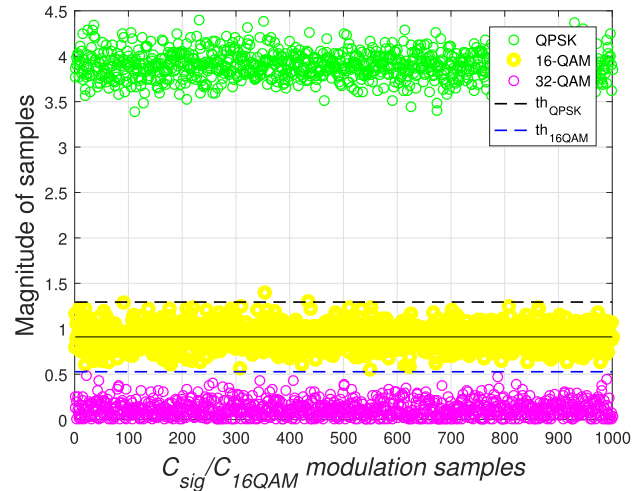
FIGURE 17. Definition of th_{qpsk} and th_{16QAM} thresholds.
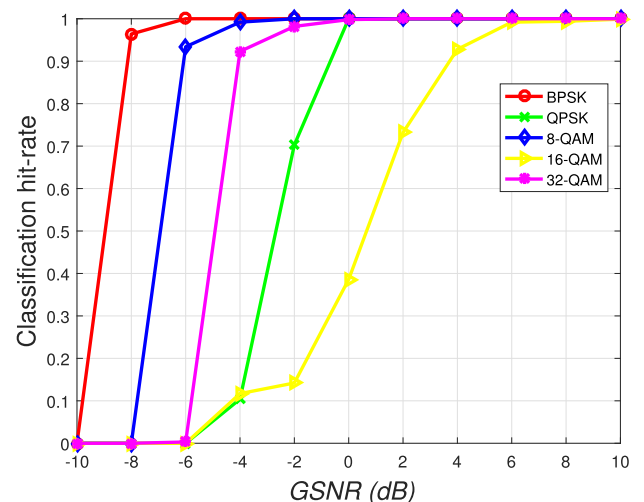
FIGURE 18. AMC using the CCF with $\sigma = 1.2$, and 1,000 interactions while varying the GSNR.

The results in Fig. 18 show that the architecture has different performances for each modulation, where the BPSK classification is the most accurate, and 16-QAM classification is the most sensitive to contamination. Even so, in the classification of BPSK, QPSK, 8-QAM, and, 32-QAM, the architecture achieves hit-rates close to 100% for GSNRs as of 0 dB. The classification of all modulations is approximately 100% when GSNR = 6 dB.

The confusion matrices of different GSNR levels are given in Tables 7 to 9 to provide a detailed analysis of the classifier. The matrices show that, for lower GSNR condition, the 16-QAM is confused with 32-QAM. This result indicates that the signature of 16-QAM, under severe noise contamination, is more approximate of the 32-QAM template than of the 16-QAM template.

Therefore, it can be inferred that the intense contamination over the 16-QAM, contributes to the fading of the cyclic component that differentiates its signature from the 32-QAM

TABLE 7. Confusion Matrix of CCF ($\sigma = 1.2$, GSNR = 0 dB).

Modulation Classification	Actual Modulation				
	BPSK	QPSK	8QAM	16QAM	32QAM
BPSK	1000	0	0	0	0
QPSK	0	1000	0	2	0
8QAM	0	0	1000	0	0
16QAM	0	0	0	386	2
32QAM	0	0	0	612	998
Below C_{th}	0	0	0	0	0

TABLE 8. Confusion Matrix of CCF ($\sigma = 1.2$, GSNR = 4 dB).

Modulation Classification	Actual Modulation				
	BPSK	QPSK	8QAM	16QAM	32QAM
BPSK	1000	0	0	0	0
QPSK	0	1000	0	1	0
8QAM	0	0	1000	0	0
16QAM	0	0	0	928	0
32QAM	0	0	0	71	1000
Below C_{th}	0	0	0	0	0

TABLE 9. Confusion Matrix of CCF ($\sigma = 1.2$, GSNR = 10 dB).

Modulation Classification	Actual Modulation				
	BPSK	QPSK	8QAM	16QAM	32QAM
BPSK	1000	0	0	0	0
QPSK	0	1000	0	1	0
8QAM	0	0	1000	0	0
16QAM	0	0	0	999	0
32QAM	0	0	0	0	1000
Below C_{th}	0	0	0	0	0

FIGURE 19. Cyclostationary signatures of QPSK modulation obtained by the FLOCAF in three different GSNR conditions.

FIGURE 20. Cyclostationary signatures of QPSK modulation obtained by the CCF in three different GSNR conditions.

signature. However, the matrices also indicate that the hit-rate of 16-QAM grows as the GSNR increases.

Directly comparing, the AMC CCF-based architecture (Fig.18) performs better than the FLOCAF-based one (Fig.14), since, considering the same channel conditions, and the same modulations, the hit-rate of CCF-based architecture is higher than hit-rate of FLOCAF-based architecture.
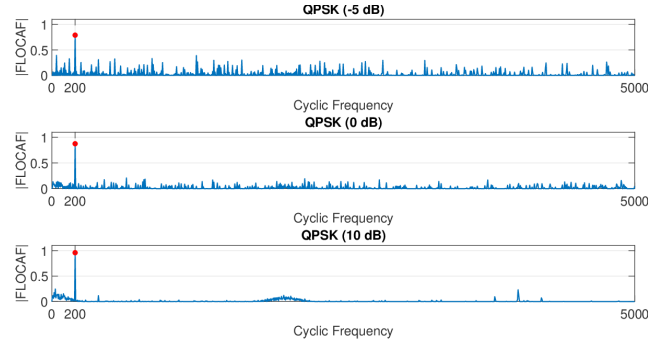
VII. SYMBOL RATE ESTIMATION

As demonstrated in section IV-B, the CCF and FLOCAF are capable of extracting cyclostationary descriptors of the modulations contaminated by alpha-stable non-Gaussian additive noise. Nevertheless, this task becomes harder at very lower GSNR levels, since the intense noise can attenuate the components from cyclostationary signatures. However, some components are more robust than others.
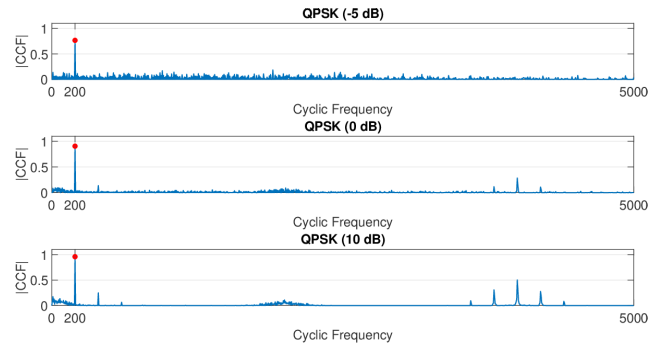
In the cyclostationary signatures provided by the FLOCAF and CCF, the component associated with the symbol rate of the modulated signal is the most robust to impulsive noise contamination, as demonstrated in Fig. 19 and Fig. 20.

Fig. 19 and Fig. 20, show the QPSK signatures generated, with the parameters presented in Table 1 from Section IV-B, by both cyclostationary functions in different GSNR conditions: -5 dB, 0 dB, and, 10 dB. In all the cases, the component associated with the symbol rate remains virtually unaltered, while the other components are fading in lower GSNR conditions.

Thus, since the cyclic component associated with the symbol rate is robust to impulsive noise contamination, moreover, considering that the intermediate frequency (f_i) is known,

and, that the symbol rate (f_b) of the signal does not exceed half of f_i, then f_b can be estimated from the signatures by the following method: the symbol rate will assume the value of the spectral position, in the range from 0 to $f_i/2$, of the cyclic component with the most significant amplitude.

Tests of the symbol rate estimation using the FLOCAF and CCF, over impulsive noise contamination, are provided as follows.
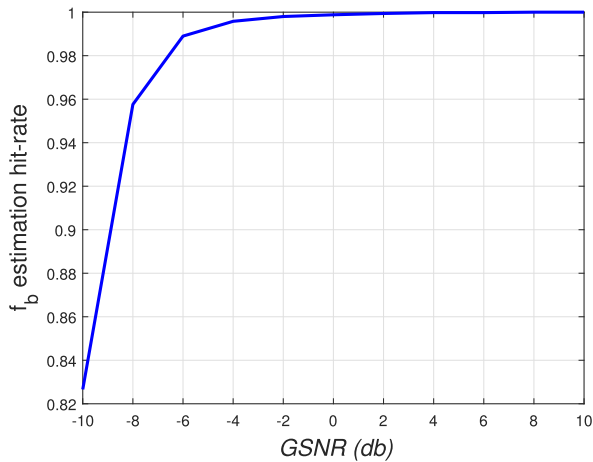
A. SYMBOL RATE ESTIMATION USING THE FLOCAF

To demonstrate that the FLOCAF, combined with the method before described in this section, enables the symbol rate estimation from modulated signals contaminated by impulsive noise, the following test was performed: first, many examples of modulations contaminated with alpha-stable noise were generated for different GSNR conditions ranging from -10 dB to 10 dB with the step of 2 dB. Then, the symbol rate estimation was performed for each instance of the signal tested.
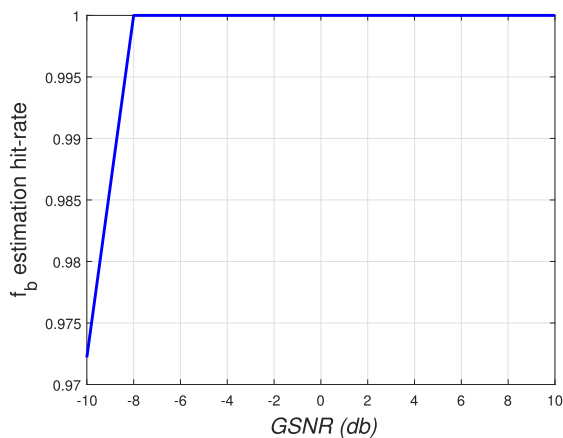
The global symbol rate estimation, which is the average among the estimation hit-rates of each modulation, was calculated considering 1,000 iterations per modulation, for each GSNR condition.

Fig. 21 shows that using FLOCAF makes it possible to obtain high accuracy levels for the estimation of symbol rates even for low GSNRs. The correct estimation, which begins above 80% in the lowest GSNR condition, increases fast and achieves a hit-rate approximately equal to 100% in GNSR = -2 dB.

FIGURE 21. Global symbol rate estimation using the FLOCAF with *a* = 0.3 and *b* = 0.5, for 1,000 interactions per modulation, for each GSNR value.

FIGURE 22. Global symbol rate estimation using the CCF with σ = 1.1, applying 1,000 interactions per modulation, for each GSNR value.

B. SYMBOL RATE ESTIMATION USING THE CCF

The same scenario, used in symbol rate estimation by FLOCAF, was applied to tests with CCF: the proposed modulations were contaminated with different alpha-stable noise levels, and the symbol rate estimation was performed for each instance of the tested signal. The global symbol rate estimation was calculated considering 1,000 iterations per modulation, in each GSNR condition.

Fig. 22 shows that with the CCF, it is possible to obtain high accuracy for the estimation of the symbol rate even for low GSNRs. The correct estimation, which begins above 97% in the lowest GSNR condition, achieve hit-rates of 100% in GSNR = −8 dB.

A directly comparing demonstrates that the estimation of the symbol rate from modulated signals, applying the CCF is more efficient than estimation using FLOCAF (Fig. 21).

VIII. CONCLUSION

This work has compared the ability of the FLOCAF and CCF to extract cyclostationary features from BPSK, QPSK, 8-QAM, 16-QAM, and, 32-QAM modulations. The obtained results allow concluding that both functions can extract unique signatures from each modulation format.

This work also has investigated the influence of the fractional lower-order parameters, *a* and *b*, and the kernel size (σ) on the performance of the AMC architectures, since they are free parameters of the FLOCAF and CCF, respectively. In this context, the numerical adjustment of FLOCAF parameters shows that the values of *a* and *b* that maximize the performance of the FLOCAF-based architecture are non-null, thus indicating that this configuration performs better than a SSCCF-based architecture. Both architectures present satisfactory behavior regarding the AMC task in impulsive environments. Notably, the CCF-based architecture achieved a superior performance than the FLOCAF-based one.

In addition to defining new AMC architectures, it has been shown that the FLOCAF and CCF can also provide the symbol rate estimation of the investigated modulations, even with high contamination by impulsive noise. In this context, the estimation based on CCF also achieved a superior performance than the FLOCAF-based symbol rate estimation.

Further studies could include the comparing of the architectures proposed in this work with new CCF-based AMC architectures combined with artificial neural networks for scenarios subjected to multipath fading and impulsive noise; besides, extend the cyclostationary analysis to higher-order digital modulations like 64-QAM and 128-QAM. Moreover, the symbol rate estimation by CCF could be integrated with an AMC architecture.

APPENDIX A
THE CCF IMPLEMENTATION

In the systems, the CCF defined in (26) can be calculated using the following estimator:

$$V_x^\epsilon(\tau) = \frac{1}{M} \sum_{m=0}^{M-1} G_\sigma(x[m], x[m+\tau])e^{-j2\pi\epsilon m}, \quad (35)$$

where $x[m]$ is a discrete-time signal, M is the number of observations, τ is a discrete-time delay and ϵ is the cyclic frequency. Although it is proven to be effective, the calculation of this estimator is directly related to the number of signal samples. In other words, the higher the value of M, the longer the processing time. Thus, the efficient calculation of CCF can be performed from the following steps:

Step 1. The input signal $x[m]$ is divided into L blocks with N samples (a given block may contain intersection samples with the previous one);

Step 2. Calculate the correntropy function $V_{x_l}(n, \tau_n)$ from each block of size N, where $n = 0, 1, 2, \ldots, N-1$ and $l = 0, 1, 2, \ldots, L-1$:

$$V_{xl}(n, \tau_n) = \frac{1}{N} \sum_{n=0}^{N-1} G_\sigma(x_l[n], x_l[n+\tau_n]); \quad (36)$$

Step 3. Calculate the mean over the blocks of correntropy function:

$$V_x(n, \tau_n) = \frac{1}{L} \sum_{l=0}^{L-1} V_{xl}(n, \tau_n); \quad (37)$$

Step 4. In order to avoid the central component that contains no cyclic information, it is necessary to centralize $V_x(n, \tau_n)$:

$$V_x(n, \tau_n) = V_x(n, \tau_n) - \frac{1}{N}\sum_{n=0}^{N-1} V_x(n, \tau_n); \quad (38)$$

Step 5. Finally, the calculation of $V_x^\epsilon(\tau)$ can be done efficiently using the Fast Fourier Transform algorithm:

$$V_x^\epsilon(\tau) = \text{fft}\{V_x(n, \tau_n)\}. \quad (39)$$

APPENDIX B
THE FLOCAF IMPLEMENTATION

The implementation of FLOCAF is similar to the CCF as described in Appendix A. Except for step 2, where $R_{xl}^{a,b}(n, \tau_n)$ in (40) is used instead of $V_{xl}(n, \tau_n)$ in (36), the remaining steps are identical.

$$R_{xl}^{a,b}(n, \tau_n) = \frac{1}{N}\sum_{n=0}^{N-1}(x_l[n]|x_l[n]|^{(a-1)})$$
$$\times(x_l[n+\tau_n]|x_l[n+\tau_n]|^{(b-1)}). \quad (40)$$

REFERENCES

[1] Z. Zhu and A. K. Nandi, *Automatic Modulation Classification: Principles, Algorithms and Applications*. Hoboken, NJ, USA: Wiley, 2014.

[2] U. Satija, B. Ramkumar, and M. S. Manikandan, "A novel sparse classifier for automatic modulation classification using cyclostationary features," *Wireless Pers. Commun.*, vol. 96, no. 3, pp. 4895–4917, 2017.

[3] H. Alharbi, S. Mobien, S. Alshebeili, and F. Alturki, "Automatic modulation classification of digital modulations in presence of HF noise," *EURASIP J. Adv. Signal Process.*, vol. 2012, no. 1, p. 238, Dec. 2012.

[4] Z. Wu, S. Zhou, Z. Yin, B. Ma, and Z. Yang, "Robust automatic modulation classification under varying noise conditions," *IEEE Access*, vol. 5, pp. 19733–19741, 2017.

[5] L. De Vito, S. Rapuano, and M. Villanacci, "Prototype of an automatic digital modulation classifier embedded in a real-time spectrum analyzer," *IEEE Trans. Instrum. Meas.*, vol. 59, no. 10, pp. 2639–2651, Oct. 2010.

[6] A. K. Nandi and E. E. Azzouz, "Algorithms for automatic modulation recognition of communication signals," *IEEE Trans. Commun.*, vol. 46, no. 4, pp. 431–436, Apr. 1998.

[7] E. Avci, D. Hanbay, and A. Varol, "An expert discrete wavelet adaptive network based fuzzy inference system for digital modulation recognition," *Expert Syst. Appl., Int. J.*, vol. 33, no. 3, pp. 582–589, Oct. 2007.

[8] E. Avci and D. Avci, "The performance comparison of discrete wavelet neural network and discrete wavelet adaptive network based fuzzy inference system for digital modulation recognition," *Expert Syst. Appl.*, vol. 35, nos. 1–2, pp. 90–101, 2008.

[9] K. Maliatsos, S. Vassaki, and P. Constantinou, "Interclass and intraclass modulation recognition using the wavelet transform," in *Proc. IEEE 18th Int. Symp. Pers., Indoor Mobile Radio Commun.*, Sep. 2007, pp. 1–5.

[10] C.-S. Park, J.-H. Choi, S.-P. Nah, W. Jang, and D. Y. Kim, "Automatic modulation recognition of digital signals using wavelet features and SVM," in *Proc. Int. Conf. Adv. Commun. Technol. (ICACT)*, Feb. 2008, vol. 1, no. 1, pp. 387–390.

[11] V. D. Orlic and M. L. Dukic, "Multipath channel estimation algorithm for automatic modulation classification using sixth-order cumulants," *Electron. Lett.*, vol. 46, no. 19, pp. 1348–1349, Sep. 2010.

[12] H.-C. Wu, M. Saquib, and Z. Yun, "Novel automatic modulation classification using cumulant features for communications via multipath channels," *IEEE Trans. Wireless Commun.*, vol. 7, no. 8, pp. 3098–3105, Aug. 2008.

[13] O. A. Dobre, A. Abdi, Y. Bar-Ness, and W. Su, "Selection combining for modulation recognition in fading channels," in *Proc. IEEE Mil. Commun. Conf.*, Oct. 2005, pp. 2499–2505.

[14] X. Zhou, Y. Wu, and B. Yang, "Signal classification method based on support vector machine and high-order cumulants," *Wireless Sensor Netw.*, vol. 2, pp. 48–52, Jan. 2010.

[15] B. Ramkumar, "Automatic modulation classification for cognitive radios using cyclic feature detection," *IEEE Circuits Syst. Mag.*, vol. 9, no. 2, pp. 27–45, 2nd Quart., 2009.

[16] K. Kim, I. A. Akbar, K. K. Bae, J.-S. Um, C. M. Spooner, and J. H. Reed, "Cyclostationary approaches to signal detection and classification in cognitive radio," in *Proc. 2nd IEEE Int. Symp. New Frontiers Dyn. Spectr. Access Netw.*, Apr. 2007, pp. 212–215.

[17] A. Fehske, J. Gaeddert, and J. H. Reed, "A new approach to signal classification using spectral correlation and neural networks," in *Proc. 1st IEEE Int. Symp. New Frontiers Dyn. Spectr. Access Netw.*, Nov. 2005, pp. 144–150.

[18] A. I. Fontes, L. A. Pasa, V. A. de Sousa, Jr., F. M. Abinader, Jr., J. A. F. Costa, and L. F. Q. Silveira, "Automatic modulation classification using information theoretic similarity measures," in *Proc. IEEE Veh. Technol. Conf. (VTC Fall)*, Sep. 2012, pp. 1–5.

[19] W. A. Gardner, *Cyclostationarity in Communications and Signal Processing*. Yountville, CA, USA: Statistical Signal Processing, 1994.

[20] W. A. Gardner, A. Napolitano, and L. Paura, "Cyclostationarity: Half a century of research," *Signal Process.*, vol. 86, no. 4, pp. 639–697, 2006.

[21] A. I. R. Fontes, J. B. A. Rego, A. D. M. Martins, L. F. Q. Silveira, and J. C. Principe, "Cyclostationary correntropy: Definition and applications," *Expert Syst. Appl.*, vol. 69, pp. 110–117, Mar. 2017.

[22] A. Tani, R. Fantacci, and D. Marabissi, "A low-complexity cyclostationary spectrum sensing for interference avoidance in femtocell LTE-A-based networks," *IEEE Trans. Veh. Technol.*, vol. 65, no. 4, pp. 2747–2753, Apr. 2016.

[23] A. Napolitano, "Cyclostationarity: New trends and applications," *Signal Process.*, vol. 120, pp. 385–408, Mar. 2016.

[24] U. Satija, M. S. Manikandan, and B. Ramkumar, "Performance study of cyclostationary based digital modulation classification schemes," in *Proc. 9th Int. Conf. Ind. Inf. Syst. (ICIIS)*, Dec. 2014, pp. 1–5.

[25] C. M. Spooner, A. N. Mody, J. Chuang, and J. Petersen, "Modulation recognition using second- and higher-order cyclostationarity," in *Proc. IEEE Int. Symp. Dyn. Spectr. Access Netw. (DySPAN)*, Mar. 2017, pp. 1–3.

[26] R. Chen, J. Wang, R. Lin, and X. Zhao, "Spectrum sensing based on nonparametric autocorrelation in wireless communication systems under alpha stable noise," *Mobile Inf. Syst.*, vol. 2016, Apr. 2016, Art. no. 6753830.

[27] M. Z. Win, P. C. Pinto, and L. A. Shepp, "A mathematical theory of network interference and its applications," *Proc. IEEE*, vol. 97, no. 2, pp. 205–230, Feb. 2009.

[28] V. A. Aalo, K. P. Peppas, G. Efthymoglou, M. Alwakeel, and S. Alwakeel, "Evaluation of average bit error rate for wireless networks with alpha-stable interference," *Electron. Lett.*, vol. 50, no. 1, pp. 47–49, Jan. 2014.

[29] M. L. de Freitas, M. Egan, L. Clavier, A. Goupil, G. W. Peters, and N. Azzaoui, "Capacity bounds for additive symmetric α-stable noise channels," *IEEE Trans. Inf. Theory*, vol. 63, no. 8, pp. 5115–5123, Aug. 2017.

[30] S. A. Bhatti, Q. Shan, I. A. Glover, R. Atkinson, I. E. Portugues, P. J. Moore, and R. Rutherford, "Impulsive noise modelling and prediction of its impact on the performance of WLAN receiver," in *Proc. 17th Eur. Signal Process. Conf.*, Aug. 2009, pp. 1680–1684.

[31] M. D. Button, J. G. Gardiner, and I. A. Glover, "Measurement of the impulsive noise environment for satellite-mobile radio systems at 1.5 GHz," *IEEE Trans. Veh. Technol.*, vol. 51, no. 3, pp. 551–560, May 2002.

[32] K. L. Blackard, T. S. Rappaport, and C. W. Bostian, "Measurements and models of radio frequency impulsive noise for indoor wireless communications," *IEEE J. Sel. Areas Commun.*, vol. 11, no. 7, pp. 991–1001, Sep. 1993.

[33] J. G. Gonzalez, J. L. Paredes, and G. R. Arce, "Zero-order statistics: A mathematical framework for the processing and characterization of very impulsive signals," *IEEE Trans. Signal Process.*, vol. 54, no. 10, pp. 3839–3851, Oct. 2006.

[34] M. Shao and C. L. Nikias, "Signal processing with fractional lower order moments: Stable processes and their applications," *Proc. IEEE*, vol. 81, no. 7, pp. 986–1010, Jul. 1993.

[35] G. A. Tsihrintzis, U. Tureli, and C. L. Nikias, "Fractional lower-order statistics-based ambiguity functions for differential delay Doppler estimation," *IEE Proc.-Radar, Sonar Navigat.*, vol. 143, no. 6, pp. 358–365, Dec. 1996.

[36] T.-H. Liu and J. M. Mendel, "A subspace-based direction finding algorithm using fractional lower order statistics," *IEEE Trans. Signal Process.*, vol. 49, no. 8, pp. 1605–1613, Aug. 2001.

[37] H. Belkacemi and S. Marcos, "Robust subspace-based algorithms for joint angle/Doppler estimation in non-Gaussian clutter," *Signal Process.*, vol. 87, no. 7, pp. 1547–1558, 2007.

[38] Y. Hu, M. Liu, C. Cao, and B. Li, "Modulation classification in alpha stable noise," in *Proc. IEEE 13th Int. Conf. Signal Process. (ICSP)*, Nov. 2016, pp. 1275–1278.

[39] J. C. Principe, *Information Theoretic Learning: Renyi's Entropy and Kernel Perspectives*. Berlin, Germany: Springer, 2010.

[40] P. Wang, T.-S. Qiu, F.-Q. Ren, and A.-M. Song, "A robust DOA estimator based on the correntropy in alpha-stable noise environments," *Digit. Signal Process.*, vol. 60, pp. 242–251, Jan. 2017.

[41] J. Lunden, S. A. Kassam, and V. Koivunen, "Robust nonparametric cyclic correlation-based spectrum sensing for cognitive radio," *IEEE Trans. Signal Process.*, vol. 58, no. 1, pp. 38–52, Jan. 2010.

[42] J. Renard, L. Lampe, and F. Horlin, "Spatial sign cyclic-feature detection," *IEEE Trans. Signal Process.*, vol. 61, no. 18, pp. 4521–4531, Sep. 2013.

[43] J. Lunden and V. Koivunen, "Spatial Sign and Rank Cyclic Detectors," *IEEE Signal Process. Lett.*, vol. 21, no. 5, pp. 595–599, May 2014.

[44] G.-H. You, T.-S. Qiu, and A.-M. Song, "Novel direction findings for cyclostationary signals in impulsive noise environments," *Circuits, Syst. Signal Process.*, vol. 32, no. 6, pp. 2939–2956, 2013.

[45] Y. Liu, T. Qiu, and J. Li, "Joint estimation of time difference of arrival and frequency difference of arrival for cyclostationary signals under impulsive noise," *Digit. Signal Process.*, vol. 46, pp. 68–80, Nov. 2015.

[46] S. Y. Luan, T. Qiu, Y. Zhu, and L. Yu, "Cyclic correntropy and its spectrum in frequency estimation in the presence of impulsive noise," *Signal Process.*, vol. 120, pp. 503–508, Mar. 2016.

[47] T. Liu, T. Qiu, and S. Luan, "Cyclic correntropy: Foundations and theories," *IEEE Access*, vol. 6, pp. 34659–34669, 2018.

[48] J.-P. Bardyn, T. Melly, O. Seller, and N. Sornin, "Iot: The era of LPWAN is starting now," in *Proc. 42nd Eur. Solid-State Circuits Conf. (ESSCIRC)*, Sep. 2016, pp. 25–30.

[49] J. Lorincz and D. Begusic, "Physical layer analysis of emerging IEEE 802.11n WLAN standard," in *Proc. 8th Int. Conf. Adv. Commun. Technol. (ICACT)*, vol. 1, Feb. 2006, p. 6 and 194.

[50] C. C. Stevenson, G. Chouinard, Z. Lei, W. Hu, S. J. Shellhammer, and W. Caldwell, "IEEE 802.22: The first cognitive radio wireless regional area network standard," *IEEE Commun. Mag.*, vol. 47, no. 1, pp. 130–138, Jan. 2009.

[51] G. A. Tsihrintzis and C. L. Nikias, "Performance of optimum and suboptimum receivers in the presence of impulsive noise modeled as an alpha-stable process," *IEEE Trans. Commun.*, vol. 43, no. 234, pp. 904–914, Feb. 1995.

[52] G. Yang, J. Wang, G. Zhang, Q. Shao, and S. Li, "Joint estimation of timing and carrier phase offsets for MSK signals in alpha-stable noise," *IEEE Commun. Lett.*, vol. 22, no. 1, pp. 89–92, Jan. 2018.

[53] G. Samorodnitsky and M. S. Taqqu, *Stable Non-Gaussian Random Processes: Stochastic Models with Infinite Variance*, vol. 1. Boca Raton, FL, USA: CRC Press, 1994.

[54] R. F. Brcich, D. R. Iskander, and A. M. Zoubir, "The stability test for symmetric alpha-stable distributions," *IEEE Trans. Signal Process.*, vol. 53, no. 3, pp. 977–986, Mar. 2005.

[55] P. G. Georgiou, P. Tsakalides, and C. Kyriakakis, "Alpha-stable modeling of noise and robust time-delay estimation in the presence of impulsive noise," *IEEE Trans. Multimedia*, vol. 1, no. 3, pp. 291–301, Sep. 1999.

[56] A. Mahmood, M. Chitre, and M. A. Armand, "PSK communication with passband additive symmetric α-stable noise," *IEEE Trans. Commun.*, vol. 60, no. 10, pp. 2990–3000, Oct. 2012.

[57] T. C. Chuah, B. S. Sharif, and O. R. Hinton, "Nonlinear decorrelator for multiuser detection in non-Gaussian impulsive environments," *Electron. Lett.*, vol. 36, no. 10, pp. 920–922, May 2000.

[58] S. Serneels, E. De Nolf, and P. J. Van Espen, "Spatial Sign Preprocessing: A simple way to impart moderate robustness to multivariate estimators," *J. Chem. Inf. Model.*, vol. 46, no. 3, pp. 1402–1409, 2006.

[59] C. Shi, Z. Dou, and L. Qi, "Distortion-constraint-based group sparse channel estimation under α-stable noise," *IEEE Access*, vol. 7, pp. 21392–21399, 2019.

[60] M. M. Mukaka, "A guide to appropriate use of correlation coefficient in medical research," *Malawi Med. J.*, vol. 24, no. 3, pp. 69–71, 2012.
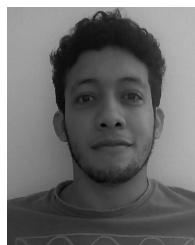
TALES V. R. O. CÂMARA received the B.S. degree in electrical engineering and the M.S. degree in mechatronics engineering from the Universidade Federal do Rio Grande do Norte (UFRN), Brazil, in 2013 and 2016, respectively, where he is currently pursuing the Ph.D. degree in electrical and computer engineering. In 2017, he was a Temporary Professor with the Department of Biomedical Engineering, UFRN. His research interests include digital signal and image processing, and communication systems.

ARTHUR D. L. LIMA received the B.S. degree in computer engineering and the M.S. degree in electrical and computer engineering from the Universidade Federal do Rio Grande do Norte (UFRN), in 2009 and 2014, respectively, where he is currently pursuing the Ph.D. degree in electrical and computer engineering. His research interests include cyclostationary signal processing, data processing, parallel software efficiency, parallel software scalability, and communication systems.

BRUNO M. M. LIMA is currently pursuing the B.Sc. degree in electrical engineering with the Universidade Federal do Rio Grande do Norte (UFRN), Natal, Brazil. His research interest includes cyclostationary signal processing.

ALUISIO I. R. FONTES received the B.S. degree in computer engineering and the M.S. and Ph.D. degrees in electrical engineering and computing from the Federal University of Rio Grande do Norte (UFRN), Natal, Brazil, in 2006, 2012, and 2015, respectively. He is currently a Professor with the Instituto Federal de Educação, Ciência e Tecnologia do Rio Grande do Norte (IFRN). His research interests include information theoretic, data processing, communication systems, and artificial intelligence.

ALLAN DE M. MARTINS received the B.Sc., M.Sc., and Ph.D. degrees in electrical engineering from the Universidade Federal do Rio Grande do Norte (UFRN), Natal, Brazil, in 2000, 2001, and 2005, respectively, where he is currently an Associate Professor. He held postdoctoral positions at the Computational Neuro-Enginering Laboratory (CNEL), Florida University, Gainesville, FL, USA, in 2006, and the Observatoire de Genéve, Geneva, Switzerland, in 2017. His research interests include digital signal and image processing, machine learning, control systems, and other related areas.

LUIZ F. Q. SILVEIRA received the B.Sc., M.Sc., and Ph.D. degrees in electrical engineering from the Universidade Federal de Campina Grande (UFCG), Campina Grande, Brazil, in 2000, 2002, and 2006, respectively. From 2006 to 2010, he was a Professor with the Instituto Federal de Educação, Ciência e Tecnologia do Rio Grande do Norte (IFRN), Natal, Brazil. Since 2010, he has been a Professor with the Department of Computing Engineering and Automation, Universidade Federal do Rio Grande do Norte (UFRN), Natal. His research interests include digital signal processing for communication systems, information-theoretic learning, channel coding, dynamic spectrum access, industrial wireless sensor networks, energy saving in data processing, and communication systems.

• • •